KSME

Springer

Journal of Mechanical Science and Technology 34 (5) 2020

Original Article
DOI 10.1007/s12206-020-0422-y

Keywords:
· Friction stir welding
· Boron steel
· Microstructure
· Transmission electron microscopy

Correspondence to:
Sung-Tae Hong
sthong@ulsan.ac.kr
Kwang-Jin Lee
kjlee@kitech.re.kr

Citation:
Das, H., Mondal, M., Hong, S.-T., Lee, K.-J., Chattopadhyay, K. (2020). Microstructure and mechanical properties evaluation of friction stir welded boron steel. Journal of Mechanical Science and Technology 34 (5) (2020) 2011~2017.
http://doi.org/10.1007/s12206-020-0422-y

Received October 22nd, 2019
Revised February 6th, 2020
Accepted March 6th, 2020

† Recommended by Editor Chongdu Cho

Microstructure and mechanical properties evaluation of friction stir welded boron steel

Hrishikesh Das[1], Mounarik Mondal[1], Sung-Tae Hong[1], Kwang-Jin Lee[2] and Kinnor Chattopadhyay[3]

[1]School of Mechanical Engineering, University of Ulsan, Ulsan, Korea, [2]Environment Materials and Components Center, Korea Institute of Industrial Technology, Jeonju, Korea, [3]Department of Materials Science & Engineering, University of Toronto, Toronto, Canada

Abstract The microstructure and mechanical properties of friction stir welded boron steel in butt joint configuration are experimentally studied. Two different friction stir welding (FSW) parameter combinations are used to successfully fabricate butt joints. Microstructural analysis exhibites that the stir zone (SZ) primarily consists of fine lath martensite, while the thermo-mechanically affected zone (TMAZ) comprises bainitic ferrite and granular bainite with a small amount of martensite. The presence of granular bainite in TMAZ suggests that alloying composition affects the phase transformation. The formation of recrystallized structures with lath martensites and high dislocation density in the SZ significantly enhance the hardness of the joints compared to that of the base metal. The results of the present study suggest that FSW can be used as a method for local hardening of structural components made of boron steels, without complicated heating and rapid cooling of a conventional hot stamping process.

1. Introduction

Automotive industries are moving towards creating vehicles with lighter weight, lower carbon footprint, and better crashworthiness. The evaluation of advanced or ultra high strength steels makes the weight reduction of automotive structures possible with ferrous alloys without compromising strength and ductility [1-4]. With the increasing use of new ferrous alloys with improved strength, automotive industries require advanced joining technologies to minimize the weakening of mechanical/material properties of joints that commonly occurs in conventional fusion joining processes.

Among the relatively new ferrous alloys, boron steels are used for hot stamping processes. In hot stamping process, boron steel has been heated just above the Ac_3 temperature (900 °C, $\gamma \rightarrow \alpha$ transition) for an appropriate dwell time to maintain homogeneous austenization. Rapid cooling after forming at elevated temperature induces the formation of martensitic phase, resulting in uniform hardening [5, 6]. Over the last decade, researchers have worked on the development of spot welding for hot-stamped boron steels. Khan et al. [7] and Ma et al. [8] observed that resistance spot weldability of hot stamped steel could be achieved by optimizing the range of the electric current. Researchers have frequently found expulsive and interfacial types of failure in resistance spot welding (RSW) of hot-stamped boron steel [7, 8]. Kim et al. [9] studied laser welding of hot stamped boron steel and observed extensive heat affected zone (HAZ) softening. HAZ softening during RSW of hot stamped boron steel was also reported by other researchers [7, 8].

Friction stir welding (FSW) [10], a solid-state joining process, is known to mitigate various issues such as the cast structure in the weld zone and HAZ softening during the joining of ferrous alloys. Miles et al. [11] investigated the microstructural phenomenon with mechanical performance of the joints for FSW of 6 mm thick DP590 steel. They concluded that acicular ferrite and

bainite formed in the stir zone (SZ) whereas, polygonal ferrite with martensite formed in the thermo-mechanically affected zone (TMAZ). Fully martensitic structure at SZ has been observed by Khan et al. [12] and Ohashi et al. [13] during friction stir spot welding (FSSW) of DP 600 steel. Santella et al. [14] reported a comparison between FSSW and RSW of bare (uncoated) and GA DP780 steel sheets. They noticed that both diffusion and mechanical interlocking/hooking phenomenon during FSSW enhanced the mechanical performance of joints compared to RSW.

Unfortunately, studies on FSW/FSSW of boron steel are still quite limited. Hovanski et al. [15] studied FSSW of hot-stamped boron steel. They observed mostly martensitic structure in the SZ and TMAZ, with a thin ferrite band at the interface of the sheets, which remained along the both sheet surfaces as well as throughout the SZ. They did not observe any HAZ softening in the joint.

Since the peak temperature during FSW/FSSW of steels can reach up to 1000-1200 °C, which is clearly above than the Ac_3 temperature of boron steel, it is expected that FSW/FSSW of boron steel without hot stamping would induce a unique microstructural change in the SZ and TMAZ. In the present study, FSW of boron steel without hot stamping is considered. The microstructural investigation and texture pattern of the joints are addressed using scanning electron microscopy (SEM), electron back scattered diffraction (EBSD), and transmission electron microscopy (TEM). The results of this microstructural analysis are then correlated with the mechanical properties from hardness measurements.

2. Experimental procedure

Boron steel sheet of 2 mm thick was used as a base material during FSW. Chemical composition of the base metal is listed in Table 1. A custom-made FSW machine (RM1, TTI, USA) was used to fabricate all the joints. The process response (axial (Z) force and torque), and the depth of penetration were simultaneously recorded for each case with an embedded DAQ system. The temperature profiles during FSW were recorded using an infrared thermal imaging camera (FLIR-T621, FLIR, Sweden). A spark plasma sintered tungsten carbide (WC) tool was used. The detailed geometry of the tool with the process parameter combinations are specified in Table 2.

To determine the successful fabrication of the joints, the cross sections were analyzed with an optical microscope (OM). Quasi-static tensile tests in the perpendicular direction to the tool travel direction were also conducted to confirm successful joining by the occurrence of failure in the base metal, which is typically used to evaluate the soundness of joining. The tensile tests were conducted with a displacement rate of 2.5 mm/min until complete failure.

For microstructural analysis, the cross section of the joints was analyzed by SEM (JEOL, JSM 7600F, Japan). EBSD (Oxford Instruments/HKL Nordlys 5 Channel) analysis was conducted to characterize the crystallographic orientation maps.

Table 1. Chemical composition of boron steel.

C	Si	Mn	Cr	B	Ti	Fe
0.2	0.2	1.18	0.02	0.004	0.004	Bal.

Table 2. FSW tool geometry and process parameters.

Tool geometry	Material	PCBN
	Shoulder diameter (mm)	14.3
	Probe length (mm)	2
	Shoulder type	Convex scrolled shoulder
Process parameter	Tool rotational speed (rpm)	1200 (P1), 1500 (P2)
	Travel speed (mm/min)	50
	Tool tilt angle (°)	2
	Depth of penetration (mm)	1.85

TEM was used to analyze the SZ and TMAZ using a microscope (JEOL-2000EX, manufacturer, Japan) operating at 200 kV. For TEM analysis, dual ion beam polishing (FEI Quanta 3D FEG Dual Beam) was used to prepare interface specimens. Microhardness was determined using Vickers microhardness indenter (HM-100, Mitutoyo, Japan), with a load of 490.5 mN and a dwell time of 10 sec, across the weld cross section.

3. Results and discussion

Fig. 1 clearly exhibits successful FSW joining of boron steel with two different combinations of parameters without any macroscopic defects. The tensile test results of FSW joints show that the failure occurred in the base metal for both process parameter sets, P1 and P2, as shown in Fig. 2.

Understanding the thermal history during FSW of boron steel helps to evaluate microstructural phenomena in detail. The temperature distribution along the perimeter of the tool shoulder showed that the maximum temperature exceeded 900 °C (Fig. 3(a)) and 1050 °C (Fig. 3(b)) for the P1 and P2 parameter sets, respectively. The temperature distribution confirms that the temperature of the material under the tool shoulder during the FSW process was clearly higher than the Ac_3 temperature (811 °C) [16] of the boron steel.

Process responses (axial force and torque) during FSW are significantly relevant to understand the consequence of thermally activated softening, deformation, and strain and strain rate hardening. Frictional heat generation increases with increasing tool rotational speed and enhancing thermal softening of the material. Fig. 4(a) shows that at a constant tool travel speed, the joining process progressed at lower axial force with higher tool rotational speed.

Evolution of the axial force is the response generated by the work piece material under the influence of processing parameters. Interestingly, it was also noted that the axial torque re-

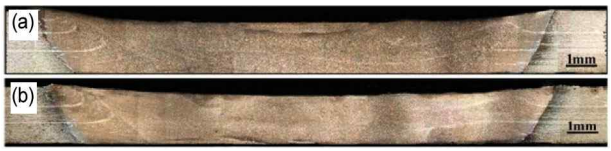

Fig. 1. Macrographs for (a) P1; (b) P2.

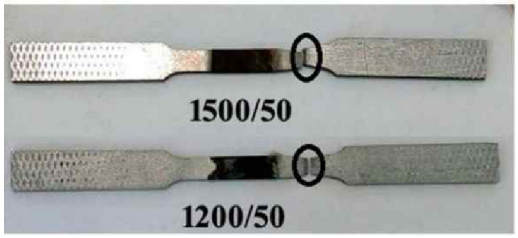

Fig. 2. Failure locations for FSW joints after tensile test.

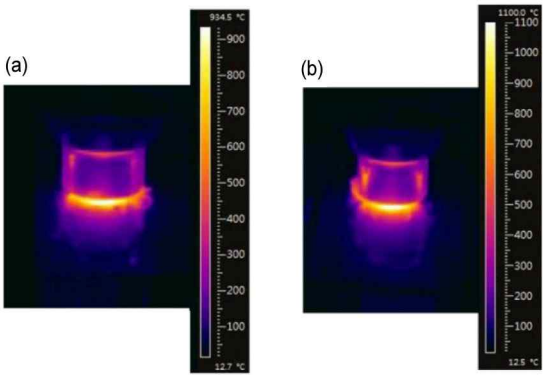

Fig. 3. Thermal camera profiles of butt welded joint for (a) 1200 rpm, 50 mm/min (P1); (b) 1500 rpm, 50 mm/min (P2) combinations of parameters.

sponse decreased with the increase in tool rotational speed (Fig. 4(b)). Reduction of the torque with increasing tool rotational speed is associated with the material flow phenomenon and the viscous characteristics of the material around the tool induced by higher heat input. The base metal microstructure showed typical ferrite and pearlite structures (Fig. 5). The microstructures of the SZ for both P1 and P2 clearly show dynamic recrystallization phenomenon with fine lath martensites, as shown in Figs. 6(a) and 7(a), respectively. Whereas, the TMAZs for both P1 (Fig. 6(b)) and P2 (Fig. 7(b)) primarily consist of bainitic ferrite/granular bainite with small amounts of martensite. EBSD analysis was conducted at the center of the SZ and the TMAZ for both P1 (Fig. 8) and P2 (Fig. 9).

The inverse pole figure (IPF) maps for P1 show that the SZ is predominantly composed of fine lath martensite (Fig. 8(a)), while the TAMZ has a bainitic structure (Fig. 8(b)). The orientation distribution functions (ODFs) of the SZ for P1 at the Φ = 45° and 65° sections of the Euler space were obtained along the standard ODF, as shown in Figs. 8(a1) and (a2), respectively. The texture exhibited strong $(001)\left[0\bar{1}0\right]$, $(111)\left[1\bar{3}2\right]$, $(110))\left[3\bar{3}2\right]$ components at Φ = 45° and a very strong S

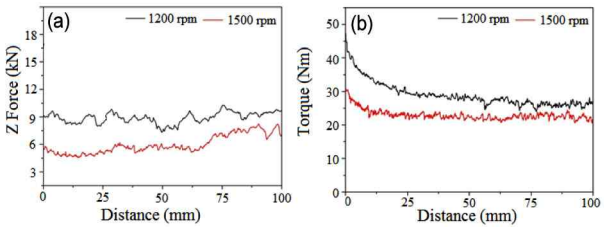

Fig. 4. (a) Z Force; (b) torque response for 1200 rpm, 50 mm/min (P1) and 1500 rpm, 50 mm/min (P2) combinations of parameters.

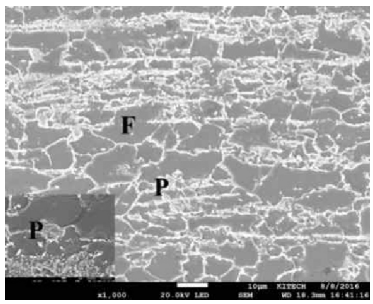

Fig. 5. Microstructure of boron steel base metal.

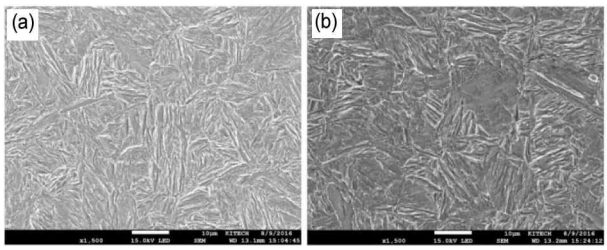

Fig. 6. SEM microstructure of P1 FS welded joint: (a) SZ; (b) TMAZ.

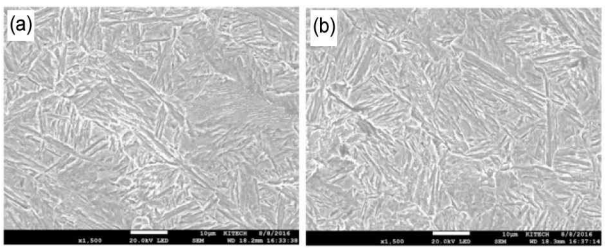

Fig. 7. SEM microstructure of P2 FS welded joint: (a) SZ; (b) TMAZ.

component $(123)\left[634\right]$ at Φ = 65° in the SZ. The main components of the texture at Φ = 45° emerged from α and γ fibers. On the other hand, the texture in the TMAZ showed only $(110)\left[1\bar{1}3\right]$, $(110)\left[3\bar{3}1\right]$, $(001)\left[\bar{2}\bar{3}0\right]$ components at Φ = 45° and no S component at Φ = 65°, as shown in Figs. 8(b1) and (b2).

The IPF map of the SZ for P2 shows slightly coarser lath martensite in comparison with that for P1, as clearly determined by comparing Figs. 9(a) and 8(a). Interestingly, it is observed that the lath structure diminished significantly in the TMAZ for both P1 and P2. The TMAZ of P2 (Fig. 9(b)) shows coarse islands of bainite and fewer laths compared to P1 (Fig.

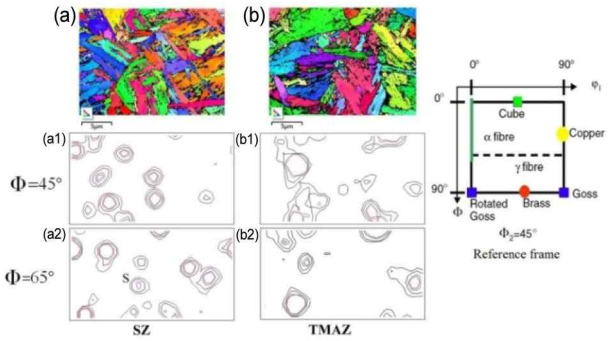

Fig. 8. P1 FS welded joint IPF maps for (a) SZ; (b) TMAZ, texture development through ODF for SZ at (a1) Φ = 45°; (a2) Φ = 65°; for TMAZ at (b1) Φ = 45°; (b2) Φ = 65°.

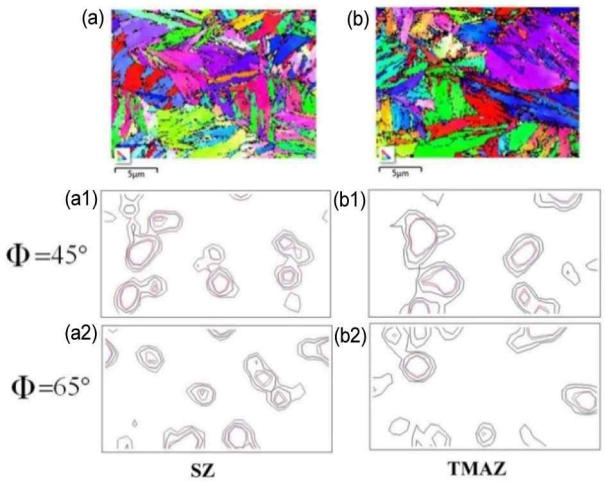

Fig. 9. P2 FS welded joint IPF maps for (a) SZ; (b) TMAZ, texture development through ODF for SZ at (a1) Φ = 45°; (a2) Φ = 65°; for TMAZ at (b1) Φ = 45°; (b2) Φ = 65°.

9b)). These results are reasonable since it is expected that the higher tool rotational speed in P2 enhanced grain growth with dynamic recrystallization and recovery. The ODFs of the SZ for P2 at the Φ = 45° and 65° sections of the Euler space were also obtained, as shown in Figs. 9(a1) and (a2), respectively. The texture exhibited strong (001) $[\bar{2}30]$, (110) $[3\bar{3}1]$, (001) $[0\bar{1}0]$ components at Φ = 45° and a very strong S component $(123)[634]$ at Φ = 65° in SZ. Whereas, the texture in the TMAZ showed (110) $[1\bar{1}3]$, (110) $[2\bar{2}1]$, (001) $[\bar{2}30]$ components at Φ = 45° and no S component at Φ = 65°, as shown in Figs. 9(b1) and (b2), respectively.

TEM analysis at the SZ for P1 clearly demonstrates the lath martensitic structure (Fig. 10(b)). Dislocation debris accumulated near the lath boundaries and recrystallized structures were observed in the SZ (Fig. 10(c)). Accumulation of dislocations adjacent to the martensite laths corresponds well with the results in Refs. [18-20]. Granular bainite and bainitic laths with a very small amount of martensite laths were observed in the

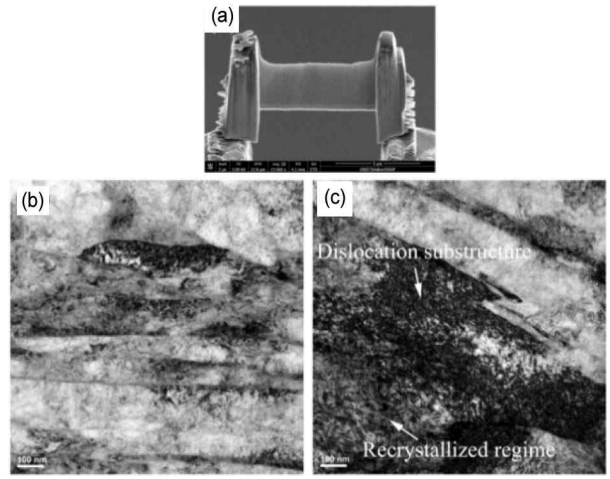

Fig. 10. (a) SZ interface sample for P1 after dual ion beam polishing, HRTEM image of P1 SZ; (b) bright field image of lath martensite; (c) dislocation substructure and recrystallized regime.

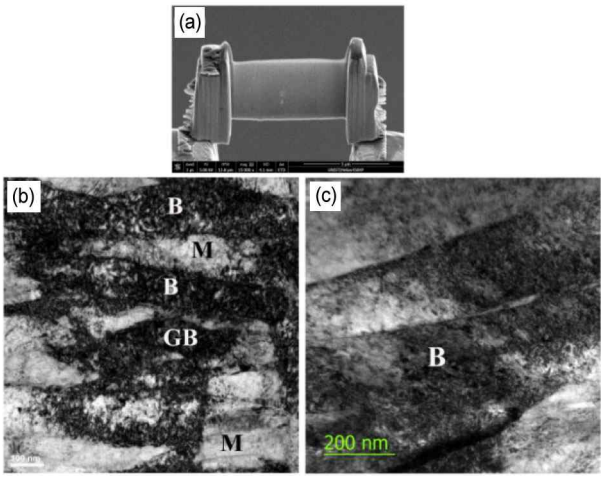

Fig. 11. (a) TMAZ interface sample for P1 after dual ion beam polishing, HRTEM image of P1 TMAZ; (b) bright field image of lath bainite, martensite and granular bainite; (c) lath bainite with dislocations.

TMAZ of P1 (Fig. 11(c)). Due to the similarity of the resultant microstructures of P1 and P2 as observed in EBSD analysis, TEM observation on the SZ and TMAZ was only conducted for P1, for the simplicity of the study.

As presented above, the severe deformation with high strain rates at the elevated temperature during FSW resulted in the complicated microstructures of the SZ and the TMAZ. During FSW, the SZ experienced temperatures around 1000-1100 ºC, which is higher than the Ac_3 temperature. On the other hand, the boron content of the boron steel hinders conversion into softer microstructures and induces a martensitic microstructure during phase transformation [20-22]. Interestingly, boron acts primarily as a hardenability element, though boron also influences the formation of granular bainite, acicular ferrite, and bainitic ferrite, in addition to martensite, depending on the deformation and cooling rate [21]. With the aid of boron content,

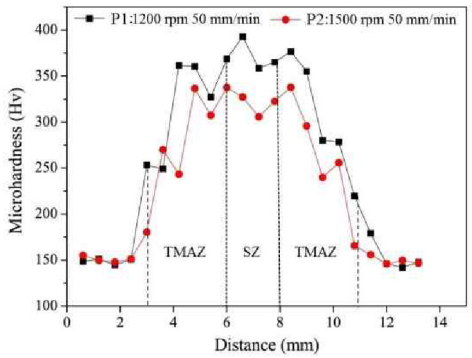

Fig. 12. Microhardness vis-à-vis distance plot.

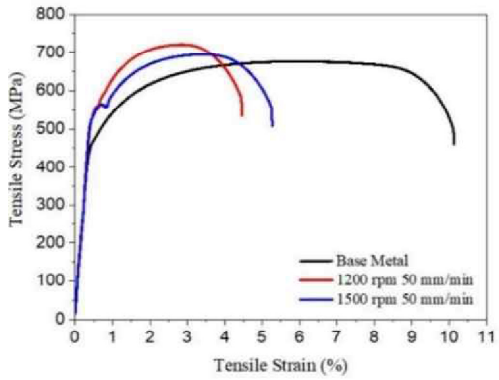

Fig. 13. Stress-strain curves.

severe deformation with very high strain rates and relatively fast cooling rates enhanced the formation of martensite over bainite in the SZ.

It is speculated that the local shear strain in the SZ during FSW, along with the effect of boron, resulted in the localized high dislocation density adjacent to martensite lath boundaries [23, 24]. The localized high dislocation density increased the driving force for recrystallization. Similar increase in dislocation density due to boron have also been observed by other researchers [22, 23].

The result of microstructural analysis suggests that the effect of boron content on the microstructural phenomenon is more prominent in the TMAZ. The formation of granular bainite along with lath bainite indicates the strong effect of boron content. Micro-alloyed boron enhanced the granular bainitic microstructure [24-27] composed of dislocated bainitic ferrites, as shown in Fig. 11(b). It is well established that deformed sub-grains and grain boundaries are the preferential sites in nucleation, thus enhancing the probability of bainitic transformation [23]. This phenomenon is clearly seen in Fig. 11(b). The larger amount of bainite over martensite in the TMAZ could be explained by that the deformation during thermo-mechanical processing with relatively slow cooling rate enhanced the formation of bainite.

The formation of recrystallized structure with martensitic laths and high dislocation density in the SZ significantly increases the microhardness (Fig. 12) compared to the base metal. For both P1 and P2, the SZ shows slightly higher hardness than the TMAZ. This is probably due to the strengthening mechanism attributed to the amount of granular/lath bainite with dislocation density within the bainitic ferrite matrix [23, 26].

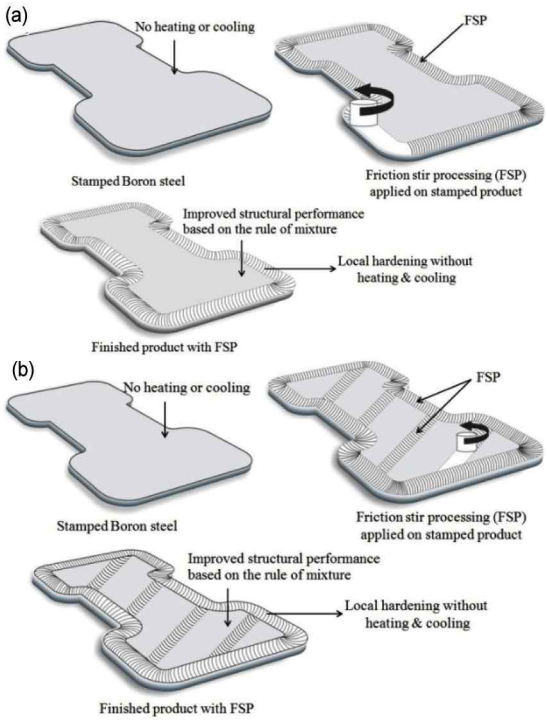

Fig. 14. Schematic of local hardening by FSW process.

The tensile test results (Fig. 13), microstructural observation, and hardness measurements consistently indicate that the FSWed zone has much higher strength than the base metal. The results suggest that FSW (or friction stir processing; FSP) can be used as a method for local hardening of structural components made of boron steel without applying a hot stamping process. For example, a center pillar of a vehicle can be directly stamped using boron steel without heating. FSW (or FSP) can then be applied locally to generate regions with higher strength, as schematically suggested in Fig. 14.

4. Conclusion

FSW of boron steel without hot stamping has been achieved successfully without any macroscopic defects. Microstructural analysis exhibited that the SZ mainly consists of fine lath martensite, while the TMAZ consists of bainitic ferrite/granular bainite with a small amount of martensite. The microstructural results suggest that the effects of alloying elements should be carefully dealt with for the development of FSW processes for high strength steels. The result of hardness measurements suggests that FSW can be used as a method for local hardening of structural components made of boron steel without complicated heating and rapid cooling, which are unavoidable during hot stamping.

Acknowledgements

This research was supported by the 2019 research fund of the University of Ulsan.

References

[1] R. G. Davies, The deformation behavior of a vanadium-strengthened dual phase steel, *Metall. Trans. A,* 9 (1) (1978) 41-52.

[2] G. Thomas and J. Y. Koo, Structure and properties of dual-phase steels, R. A. Kot and J. W. Morris(eds.), *TMS-AIME*, New York, NY (1979) 183.

[3] S. K. Paul, Real microstructure based micromechanical model to simulate microstructural level deformation behavior and failure initiation in DP 590 steel, *Mater. Des.,* 44 (2013) 397-406.

[4] M. Pouranvari and S. P. H. Marashi, Critical review of automotive steels spot welding: Process, structure and properties, *Sci. Technol. Weld. Join.,* 18 (5) (2013) 361-403.

[5] K. A. Dinh, S.-T. Hong, T. V. Luu, M. J. Kim and H. N. Han, Intermetallic evolution of Al-Si-coated hot stamping steel during modified electrically assisted rapid heating, *Acta Metall. Sinica*., 31 (12) (2018) 1327-1333.

[6] H. Karbasian and A. E. Tekkaya, A review on hot stamping, *J. Mater. Proc. Tech*., 210 (15) (2010) 2103-2118.

[7] M. S. Khan, S. D. Bhole, D. L. Chen, G. Boudreau, E. Biro and J. V. Deventer, Welding behaviour, microstructure and mechanical properties of dissimilar resistance spot welds between galvannealed HSLA350 and DP600 steels, *Sci. Technol. Weld. Join.,* 14 (7) (2009) 616-625.

[8] C. Ma, D. L. Chen, S. D. Bhole, G. Boudreau, A. Lee and E. Biro, Microstructure and fracture characteristics of spot-welded DP600 steel, *Mater. Sci. Eng. A,* 485 (1-2) (2008) 334-346.

[9] C. Kim, M. J. Kang and Y. D. Park, Laser welding of Al-Si coated hot stamping steel, *Proc. Eng*., 10 (2011) 2226-2231.

[10] W. M. Thomas, E. D. Nicholas, J. C. Needham, M. G. Murch, P. Templesmith and C. J. Dawes, Friction stir butt welding, *Int. Patent App. PCT/GB92/02203 and G.B. Patent App. 9125978. 8* (1991).

[11] M. P. Miles, T. W. Nelson, R. Steel, E. Olsen and M. Gallagher, Effect of friction stir welding conditions on properties and microstructures of high strength automotive steel, *Sci. Technol. Weld. Join*., 14 (3) (2009) 228-232.

[12] M. I. Khan, M. L. Kuntz, P. Su, A. Gerlich, T. North and Y. Zhou, Resistance and friction stir spot welding of DP600: A comparative study, *Sci. Technol. Weld. Join*., 12 (2) (2007) 175-182.

[13] R. Ohashi, Study on friction stir spot welding of dual-phase high-strength steel sheets, *Weld. World,* 55 (2011) 21-26.

[14] M. Santella, Y. Hovanski, A. Frederick, G. Grant and M. Dahl, Friction stir spot welding of DP780 carbon steel, *Sci. Technol, Weld. Join*., 15 (4) (2010) 271-278.

[15] Y. Hovanski, M. L. Santella and G. J. Grant, Friction stir spot welding of hot-stamped boron steel, *Scrip. Mater*., 57 (9) (2007) 873-876.

[16] M. Zhang, Z. Wan and L. Li, Transformation characteristics and properties of B steel 22MnB5, *Mater. Today: Proceed*., 2S (2015) S697 S700.

[17] H. Das, M. Mondal, S.-T. Hong, Y. Lim and K. J. Lee, Comparison of microstructural and mechanical properties of friction stir spot welded ultra-high strength dual phase and complex phase steels, *Mater. Character*., 139 (2018) 428-436.

[18] T. Furuhara, T. Chiba, T. Kaneshita, H. Wu and G. Miyamoto, Crystallography and interphase boundary of martensite and bainite in steels, *Metall. Mat. Trans. A,* 48 (6) (2017) 2739-2752.

[19] A. Shibata, T. Furuhara and T. Maki, Interphase boundary structure and accommodation mechanism of lenticular martensite in Fe-Ni alloys, *Acta. Mater.,* 58 (9) (2010) 3477-3492.

[20] X. P. Shen and R. Priestner, Effect of boron on the microstructure and tensile properties of dual-phase steel, *Met. Mat. Trans. A,* 21A (9) (1990) 2547-2553.

[21] G. F. Melloy, P. R. Slimmon and P. P. Podgursky, Optimizing the boron effect, *Met. Mat. Trans. A,* 4 (10) (1973) 2279-2289.

[22] M. Nikravesha, M. Naderib and G. H. Akbaria, Influence of hot plastic deformation and cooling rate on martensite and bainite start temperatures in 22MnB5 steel, *Mater. Sci. Eng. A,* 540 (2012) 24-29.

[23] J. Wang, P. J. V. Wolk and S. V. Zwaag, On the influence of alloying elements on the bainite reaction in low alloy steels during continuous cooling, *J. Mater. Sci*., 35 (17) (2000) 4393-4404.

[24] T. Song and B. C. De Cooman, Effect of boron on the isothermal bainite transformation, *Met. Mat. Trans. A,* 44A (2013) 1686-1705.

[25] H. K. D. H. Bhadeshia, *Bainite in Steels: Transformation, Microstructure and Properties*, IOM Communications Ltd., U.K. (2001) 129-188.

[26] K. Zhu, C. Oberbillig, C. I. Musik, D. Loison and T. Iung, Effect of B and B + Nb on the bainitic transformation in low carbon steels, *Mater. Sci. Eng. A*, 528 (2011) 4222-4231.

[27] C. A. Siebert, D. V. Doane and D. H. Breen, The hardenability of steels - Concepts, metallurgical influence and industrial applications, *American Society for Metals* (1977) 72-129.

Hrishikesh Das is a Post-doctorate Researcher in the School of Mechanical Engineering, University of Ulsan. His research interest is friction stir welding.

Mounarik Mondal is a Ph.D. candidate in the School of Mechanical Engineering, University of Ulsan. His research interest is friction stir welding.

Sung-Tae Hong is a Professor in the School of Mechanical Engineering, University of Ulsan. His research interest is solid state joining and advanced metal forming.

Kinnor Chattopadhyay is a Professor in the Department of Materials Science & Engineering, University of Toronto, Canada. His research interest is process metallurgy.

Kwang-Jin Lee is a Principal Researcher in KITECH, South Korea. His research interest is friction stir welding.